Radiation-Hydrodynamic Simulations of Core-collapse Supernovae with 6 Dimensional Boltzmann Neutrino Transport

IOP Conf. Series: Journal of Physics: Conf. Series **1225** (2019) 012003 doi:10.1088/1742-6596/1225/1/012003

Radiation-Hydrodynamic Simulations of Core-collapse Supernovae with 6 Dimensional Boltzmann Neutrino Transport

Hiroki Nagakura[1,2], Shun Furusawa[3], Hajime Togashi[4], Kohsuke Sumiyoshi[5] and Shoichi Yamada[6]

[1]Department of Astrophysical Sciences, Princeton University, Princeton NJ 08544
[2]TAPIR, Walter Burke Institute for Theoretical Physics, Mailcode 350-17, California Institute of Technology, Pasadena, CA 91125, USA
[3]Interdisciplinary Theoretical and Mathematical Sciences Program (iTHEMS), RIKEN 2-1 Hirosawa, Wako, Saitama 351-0198, Japan
[4]Nishina Center for Accelerator-based Science, RIKEN 2-1 Hirosawa, Wako, Saitama 351-0198, Japan
[5]Numazu College of Technology, Ooka 3600, Numazu, Shizuoka 410-8501, Japan
[6]Advanced Research Institute for Science & Engineering, Waseda University, 3-4-1 Okubo, Shinjuku, Tokyo 169-8555, Japan

E-mail: [1]hirokin@caltech.edu

Abstract. Core-collapse supernovae (CCSNe) are intrinsically multi-scale, multi-physics and multi-dimensional phenomena. Because of the enormous complexity, the first-principles numerical simulations under realistic input physics are strongly required to uncover the explosion mechanism, predict observational signals (neutrinos, gravitational waves and electromagnetic waves) and prove physical state in extremely hot and dense matter of supernova core. We have tackled the development of multi-dimensional radiation-hydrodynamic code with full Boltzmann neutrino transport and performed several scientific CCSNe simulations in the last few years. In this article, we report the recent progress of our CCSNe numerical simulations with the most up-to-date equation-of-state (EOS) and nuclear weak interactions. We also present preliminary results of non-rotating CCSNe simulations in spatial axisymmetry.

1. Introduction

The explosion mechanism of core-collapse supernova (CCSN) is one of long-standing problems in our universe. CCSNe are intrinsically multi-scale, multi-physics and multi-dimensional phenomena with there being a complex interplay of all four fundamental forces in nature. First-principle numerical simulations are the most promising approach to reveal the nature of the explosion mechanism. They have made rapid progress with ever increasing computational resources in the last few years. Indeed, nowadays sophisticated three-dimensional CCSNe simulations can be carried out with sufficient long-term in post-bounce phase [1, 2, 3, 4, 5, 6, 7] and some of these simulations demonstrated the success of shock revival. In addition to this, under axisymmetry in space, CCSNe simulations with full Boltzmann neutrino transport are also possible on $\sim$ 10 PFLOPS supercomputer facilities and our group achieved such simulations [8]. We keep improving our code towards general relativistic three-dimensional

CCSNe simulations with full Boltzmann neutrino transport, which will be performed in the exa-scale era of computational facilities.

Nuclear equation of states (EOSs) and weak interactions in hot and densed matter are other key ingredients for core-collapse supernovae (CCSNe). Thermodynamical quantities given by EOS play a primary role for hydrodynamics. Weak interactions also dictate exchanging energy, momentum and leptons between neutrinos and matter, which affect the dynamics of CCSNe. On the other hand, accurate treatments of EOS and weak interactions on CCSNe simulations are very challenging issues, for instance, we have not yet fully undersood the property at supranuclear densities at the moment due to many difficulties on theories, observations and experiments (see a recent review by [9]); the description of nuclear abundances relevant to CCSNe has not yet been well established due to the appearance of extremely heavy nuclei where no experimental data are available. The ambiguity of nuclear state obscures the effect of neutrino-nucleus interactions, which implicitly but significantly influence on CCSNe.

Very recently, we improved the input physics by developing self-consistent treatments of nuclear EOS and weak interactions. We employ an up-to-date EOS whose uniform matter is computed based on the variational method with including realistic nuclear force. For inhomogeneous nuclear matter, the full ensemble nuclei are taken into account with various finite-density and thermal effects. The abundance of nuclei is used to compute reaction rates of nuclear weak interactions such as electron captures of heavy nuclei and electron and positron captures of light nuclei. In this article, we briefly report the essence of these improvements and then present recent results of CCSNe simulations with incorporating these improvements.

2. Multi-nuclear VM EOS

In this section, we describe the essence of physics in multi-nuclear variational method (VM) EOS. The free energy density is calculated with the variational many-body theory. The Hamiltonian consists of the kinetic, the AV18 two-body potential [10] and the UIX three-body potential [11, 12] terms. This formulation is extended to non-uniform nuclear matter at sub-nuclear densities to compute the free energy density of unbound nucleons that drip from heavy nuclei, $f_{n,p}$, as well as the bulk energies of heavy nuclei, E_{AZ}^{bulk}. The free energy density of non-uniform nuclear matter is given by

$$\begin{aligned} f &= \eta f_{n,p} + \sum_{AZ} n_{AZ} \times \\ &\quad \left\{ \kappa T \left[\ln \left(\frac{n_{AZ}}{g_{AZ}(M_{AZ}T/2\pi\hbar^2)^{3/2}} \right) - 1 \right] + M_{AZ} \right\}, \end{aligned} \tag{1}$$

where n_{AZ}, M_{AZ}, and g_{AZ} are the number density, mass, and internal degrees of freedom for nucleus with the mass number A and atomic number Z. The excluded volume effects for nucleons and nuclei are defined as $\eta = 1/[1 - \sum_{AZ}(n_{AZ}A/n_{sAZ})]$ and $\kappa = n_B/n_0$, respectively. The quantities n_0 is the nuclear saturation density of symmetric matter. We also take into account the dependencies of iso-spin of each nucleus, Z/A, and temperature on the saturation densities of heavy nuclei, n_{sAZ}.

The mass model for heavy nuclei with atomic numbers $6 \leq Z \leq 1000$ and mass numbers $A \leq 2000$ is expressed as

$$M_{AZ} = E_{AZ}^{bulk} + E_{AZ}^{surf} + E_{AZ}^{Coul} + E_{AZ}^{shell}. \tag{2}$$

The surface energy E_{AZ}^{surf} and Coulomb energy E_{AZ}^{Coul} depend on number densities of uniformly-distributed dense electrons, dripped nucleons and on shape changes of heavy nuclei from normal droplets to bubbles just below nuclear normal density. The shell energies of heavy nuclei E_{AZ}^{shell},

which represent microscopic effects such as neutron- and proton-magic numbers and pairing, are taken from the experimental and theoretical mass data [13, 14]. The temperature dependencies of E_{AZ}^{shell} and g_{AZ} are also phenomenologically taken into account. The mass model of the light nuclei with $Z < 6$ is given by $M_{AZ} = M_{data} + \Delta E_{AZ}^{Coul} + \Delta E_{AZ}^{Pauli} + \Delta E_{AZ}^{self}$ where M_{data} is the experimental mass, ΔE_{AZ}^{Coul} is Coulomb energy shift, and a quantum approach is incorporated to evaluate Pauli-energy shift ΔE_{AZ}^{Pauli} and self-energy shift ΔE_{AZ}^{self}.

3. Electron and positron captures

We calculate weak interaction rates of nuclei which are evaluated under the consistent treatment with the nuclear abundances provided by the EOS. For some nuclei, we use the reaction data in [15, 16, 17, 18], which are based on the shell model or its extension. It should be noted, however, that these theoretical computations do not cover the full nuclei which appear in CCSNe. We adopt an analytical formula as a function of the Q-value [16] for the neutron-rich and/or heavy nuclei with the unavailable data:

$$\lambda_{AZ} = \frac{(\ln 2)B}{K}\left(\frac{T}{m_e c^2}\right)^5 \times \left[F_4(\eta_{AZ}) - 2\chi_{AZ}F_3(\eta_{AZ}) + \chi_{AZ}^2 F_2(\eta_{AZ})\right], \quad (3)$$

where $K = 6146$ sec, $\chi_{AZ} = (Q_{AZ} - \Delta E)/T$, $\eta_{AZ} = (\mu_e + Q_{AZ} - \Delta E)/T$ with the electron chemical potential μ_e, and F_k is the relativistic Fermi integrals of order k. The Q-value is defined as $Q_{AZ} = M_{AZ} - M_{A,Z-1}$, where the finite temperature and density effects on the nuclear masses given by Eq. (2) are included with being consistent with the nuclear abundances on EOS tables. We use the detailed balance relation to evaluate the rate of neutrino absorption on heavy nuclei.

As for light nuclei, we include the following weak interactions in our simulation, referring to [19],

$$\text{(elpp)}: \quad \nu_e + {}^2\text{H} \longleftrightarrow e^- + p + p, \quad (4)$$
$$\text{(ponn)}: \quad \bar{\nu_e} + {}^2\text{H} \longleftrightarrow e^+ + n + n, \quad (5)$$
$$\text{(el2h)}: \quad \nu_e + n + n \longleftrightarrow e^- + {}^2\text{H}, \quad (6)$$
$$\text{(po2h)}: \quad \bar{\nu_e} + p + p \longleftrightarrow e^+ + {}^2\text{H}, \quad (7)$$
$$\text{(el3he)}: \quad \nu_e + {}^3\text{H} \longleftrightarrow e^- + {}^3\text{He}, \quad (8)$$
$$\text{(po3h)}: \quad \bar{\nu_e} + {}^3\text{He} \longleftrightarrow e^+ + {}^3\text{H}. \quad (9)$$

For neutrino absorptions on deuterons of Eqs. (4) and (5), we use the data of vacuum cross section [20]. To account for the medium modification on deuteron mass such as ΔE_{AZ}^{Coul}, ΔE_{AZ}^{Pauli}, and ΔE_{AZ}^{self}, we introduce the shifted neutrino injection energies as $E_\nu^* = E_\nu + m_{^2\text{H}}^* - m_{^2\text{H}}$ with masses of deuteron in medium, $m_{^2\text{H}}^*$, and in vacuum, $m_{^2\text{H}}$. The in-medium mass is evaluated by the same mass model in the EOS. As an example, the neutrino absorption rate of Eq. (4) is expressed as

$$1/\lambda(E_\nu) = n_{^2\text{H}} \int \mathrm{d}p_e \left[\frac{\mathrm{d}\sigma_{\nu^2\text{H}}}{\mathrm{d}p_e}[E_\nu^*)\right](1 - f_e(E_e)], \quad (10)$$

where $n_{^2\text{H}}$ is deuteron number density and f_e denotes the Fermi-Dirac distribution of electrons. The rate of the electron/positron capture on two nucleons forming a deuteron (leftward reactions of Eqs. (4) and (5)) can be evaluated through the detailed balance with the rate of the absorption.

Electron captures on deuterons of Eqs. (6) and (7) can be estimated with the assumption that the matrix elements of electron and positron captures are equivalent to those of neutrino absorptions for Eqs. (4) and (5) as

$$\frac{\mathrm{d}\sigma_{e^2\text{H}}}{\mathrm{d}p_\nu} \sim \frac{1}{2}\frac{\mathrm{d}\sigma_{\nu^2\text{H}}}{\mathrm{d}p_e}, \quad (11)$$

where $\frac{1}{2}$ comes from the difference in spin degrees of freedom between neutrino and electron. This is a reasonable approximation for CCSNe conditions, in which injection energies of leptons are not greatly large and, hence, the energy deposit to the relative motion between two nucleons is negligible. Three bound nucleons, ^{3}H and ^{3}He, interact with neutrinos via breakup or charge exchange, the latter of which is dominant neutrino opacity source. Therefore, we treat only the charge exchange reaction as described in Eqs. (8) and (9). Those rates are calculated as

$$1/\lambda(E_\nu) = n_{^3\mathrm{H}} \left[\frac{G_F^2 V_{ud}^2}{\pi(\hbar c)^4}\right] p_e E_e [1 - f_e(E_e)] B(GT), \tag{12}$$

where $n_{^3\mathrm{H}}$ is triton number density, $B(GT) = 5.87$, and $V_{ud} = 0.967$. Here, in-medium effects on nuclear masses are not taken into account.

4. Full Boltzmann code for CCSNe

All simulations presented in this article are performed by our multi-dimensional (multi-D) neutrino-radiation-hydrodynamic code [21, 22]. We solve Boltzmann equations for neutrino transport. The basic equation of our Boltzmann solver starts with the conservative form of the Boltzmann equation in general relativity:

$$\begin{aligned}
&\frac{1}{\sqrt{-g}} \frac{\partial}{\partial x^\alpha}\Big|_{q_i} \left[\left(e^\alpha_{(0)} + \sum_{i=1}^{3} \ell_i e^\alpha_i\right)\sqrt{-g} f\right] \\
&-\frac{1}{\nu^2}\frac{\partial}{\partial \nu}(\nu^3 f \omega_{(0)}) + \frac{1}{\sin\bar{\theta}}\frac{\partial}{\partial \bar{\theta}}(\sin\bar{\theta} f \omega_{(\bar{\theta})}) \\
&+\frac{1}{\sin^2\bar{\theta}}\frac{\partial}{\partial \bar{\phi}}(f\omega_{(\bar{\phi})}) = S_{\mathrm{rad}},
\end{aligned} \tag{13}$$

where g, x^α are the determinant of the metric, coordinates of space-time, respectively, and f is the neutrino distribution function; $e^\alpha_{(\mu)} (\mu = 0, 1, 2, 3)$ denote a set of the tetrad bases for a local orthonormal frame; ℓ_i are directional cosines for the direction of neutrino propagation with respect to $e^\alpha_{(i)}$. The three components of ℓ_i can be written as

$$\begin{aligned}
\ell_{(1)} &= \cos\bar{\theta}, \\
\ell_{(2)} &= \sin\bar{\theta}\cos\bar{\phi}, \\
\ell_{(3)} &= \sin\bar{\theta}\sin\bar{\phi},
\end{aligned} \tag{14}$$

where $\bar{\theta}$ and $\bar{\phi}$ stand for the polar and azimuthal angles. We further define coordinates q_i in momentum space- $q_1 = \nu, q_2 = \bar{\theta}$ and $q_3 = \bar{\phi}$ with ν being the neutrino energy in this local orthonormal frame and also expressed as $\nu \equiv -p_\alpha e^\alpha_{(0)}$ with the four momentum of neutrino, p^α. In this paper neutrinos are assumed to be massless. $\omega_{(0)}, \omega_{(\bar{\theta})}, \omega_{(\bar{\phi})}$ are given as

$$\begin{aligned}
\omega_{(0)} &\equiv \nu^{-2} p^\alpha p_\beta \nabla_\alpha e^\beta_{(0)}, \\
\omega_{(\bar{\theta})} &\equiv \sum_{i=1}^{3} \omega_i \frac{\partial \ell_{(i)}}{\partial \bar{\theta}}, \\
\omega_{(\bar{\phi})} &\equiv \sum_{i=2}^{3} \omega_i \frac{\partial \ell_{(i)}}{\partial \bar{\phi}}, \\
\omega_i &\equiv \nu^{-2} p^\alpha p_\beta \nabla_\alpha e^\beta_{(i)}.
\end{aligned} \tag{15}$$

These ω's can be expressed with the Ricci rotation coefficients. $S_{\rm rad}$ on the right hand side of Eq. (13) originates from the collision term for neutrino-matter interactions.

In the 3+1 formulation of GR, the line element is expressed as

$$ds^2 = (-\alpha^2 + \beta^k\beta_k)dt^2 + 2\beta_i dt dx^i + \gamma_{ij}dx^i dx^j, \tag{16}$$

where α, β^i and γ_{ij} denote the lapse function, shift vector and spatial 3-metric, respectively. In our extended Boltzmann code, the time-like basis $e^\alpha_{(0)}$ is chosen so that it should coincide with the unit vector n^α normal to the spatial hypersurface with $t =$ const. This choice is a natural extension from our previous SR Boltzmann solver. Then three other spatial tetrad bases are taken so that they should be tangential to the spatial hypersurface. In this paper we assume that the space-time is flat and is foliated with flat spatial hypersurfaces, on which we deploy the polar coordinates $(x^1 = r, x^2 = \theta, x^3 = \phi)$. Then non-vanishing components of the 3 metric are $\gamma_{rr} = 1, \gamma_{\theta\theta} = r^2$ and $\gamma_{\phi\phi} = r^2 \sin\theta^2$. The spatial tetrad bases are chosen so that the $e_{(1)}$ be parallel to the radial coordinate, and $e_{(2)}$ be tangential to the surface spanned by ∂_t and ∂_θ, and $e_{(3)}$ be orthogonal to the other two:

$$\begin{aligned}
e^\alpha_{(1)} &= (0, \gamma_{rr}^{-1/2}, 0, 0) \\
e^\alpha_{(2)} &= \left(0, -\frac{\gamma_{r\theta}^{-1/2}}{\sqrt{\gamma_{rr}(\gamma_{rr}\gamma_{\theta\theta} - \gamma_{r\theta}^2)}}, \sqrt{\frac{\gamma_{rr}}{\gamma_{rr}\gamma_{\theta\theta} - \gamma_{r\theta}^2}}, 0\right) \\
e^\alpha_{(3)} &= \left(0, \frac{\gamma^{r\phi}}{\sqrt{\gamma^{\phi\phi}}}, \frac{\gamma^{\theta\phi}}{\sqrt{\gamma^{\phi\phi}}}, \sqrt{\gamma^{\phi\phi}}\right).
\end{aligned} \tag{17}$$

We employ the central scheme for numerically solving the Newtonian hydrodynamic equations (see also [23]). The direct method of matrix inversion are employed to solve Poisson equation of Newtonian gravity. For all simulations, we employ the same weak interaction rates as those used in [8] except for electron and positron captures on nuclei. In our simulations, we cover the spatial domain of $0 \leq r \leq 5000$km by spherical polar coordinate. We deploy 384 grid points for radial direction and 128 grid points for lateral direction. In momentum space of neutrinos, we use 20, 10 and 6 grid points for energy ($0 \leq \epsilon \leq 300$MeV), lateral angular grid ($0^\circ \leq \bar{\theta} \leq 180^\circ$) and azimuthal angular grid in neutrino momentum space, respectively. In this study, we employ 11.2 solar masses progenitor in [24].

5. Result

The shock wave produced at core bounce expands rather gradually with time, but the prompt convection pushes the shock wave further outward. The increase of shock radius enhances the neutrino heating, which further accelerates the shock expansion. As shown in Figure 1, multi-dimensional fluid instabilities such as neutrino driven convection and standing accretion shock instability (SASI) distorts the post-shock flow and then the morphology of post-shock flows is much different from spherical symmetry. Around $t \sim 150$ms the shock wave goes through rapid expansion in the north side due to kinetic attack by turbulent motions behind the shock wave, and then it reaches in $r \sim 600$km around $t \sim 200$ms (see Figure 2).

Overall dynamics is very similar as LS model in [8] which also shows the sign of shock revival. Our results also share with other CCSNe simulations the qualitative trend that s11.2 progenitor explodes more easily than other more massive progenitors. It is important to emphasize that the inner structure of proto-neutron star (PNS) is different from those of LS model [8]. We also find that weak interactions between neutrinos and light nuclei quantitatively affect both neutrino cooling and heating. More detailed analysis of these effects are currently underway which will be presented in the forthcoming paper.

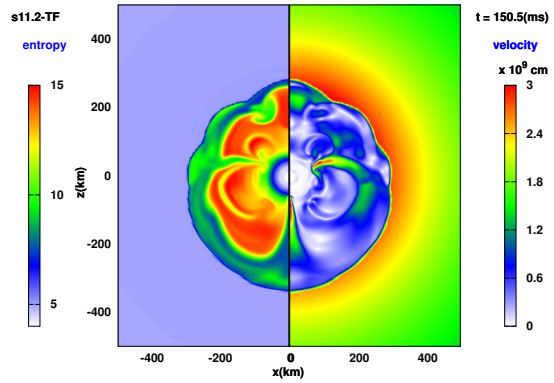

Figure 1. Entropy (left) and velocity (right) map at $t = 150$ms after bounce.

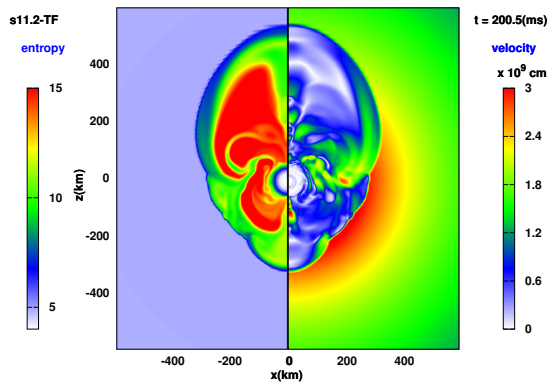

Figure 2. Same as Figure 1 but for $t = 200$ms after bounce.

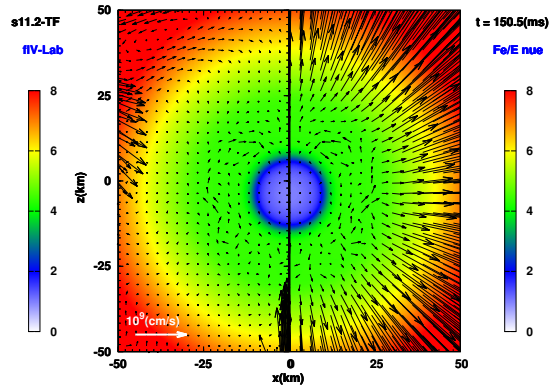

Figure 3. Entropy contour with fluid velocity vector (left) and electron-type neutrino flux vector (right) at $t = 150$ms after bounce.

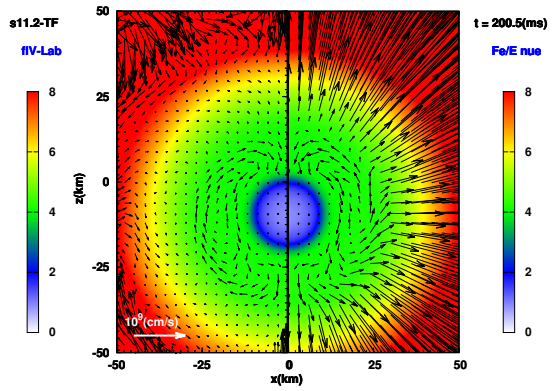

Figure 4. Same as Figure 3 but for $t = 200$ms after bounce. The offset of PNS can be clearly seen.

Although the global shock dynamics is similar as LS model in [8], we obtain a new phenomenon in this simulation, which is a recoil of PNS. The recoil of PNS can be seen by comparing between Figures 3 and 4. As mentioned before, the shock wave expands rapidly in the north side, which gives a linear momentum to PNS towards south side. In our CCSNe code the shift vector is utilized to specify the movement of spatial coordinates so that they could track the PNS motion approximately (see [22] in more details).

Although the detailed analysis of PNS recoil is currently underway, the asymmetric gravitational field gives the driving force of the kick. The asymmetric neutrino pressure in the optically thick region also play an important role to determine the acceleration of PNS, meanwhile other previous simulations took ad-hock prescriptions inside of PNS. Thanks to the moving mesh technique, we self-consistently treat both global asymmetry of shock expansion and a recoil of PNS. It should be noted however, our CCSNe simulations do not guarantee a conservation of total linear momentum. We are currently improve our code in order to reduce a violation of linear momentum, which will be also presented in the forth coming paper.

6. Summary

In this article, we make a report of our recent progress of CCSNe project. We substantially improve the input physics such as nuclear EOS and weak interactions recently and then perform spatially axisymmetric simulations of 11.2 solar masses progenitor. We find that the shock wave expands with $\ell = 1$ asymmetry which triggers the recoil of PNS. The recoil of PNS can be consistently handled by our moving mesh technique in full Boltzmann radiation-hydrodynamic code. The moving mesh technique is developed based on the 3+1 formalism of general relativistic Boltzmann equation, indeed, we make use of shift gauge to trace the motion of PNS. Our result is the first evidence of appearance of PNS recoil in CCSNe simulations with elaborate input physics and sophisticated treatment of neutrino transport. The recoil of PNS would generate the asymmetric neutrino radiation and may affect the shock expansion in CCSNe, all of which are currently analyzed in detail and will be reported in our forthcoming papers.

References

[1] T. Takiwaki, K. Kotake and Y. Suwa, Astrophys. J. **749**, 98 (2012) doi:10.1088/0004-637X/749/2/98 [arXiv:1108.3989 [astro-ph.HE]].
[2] E. J. Lentz *et al.*, Astrophys. J. **807**, no. 2, L31 (2015) doi:10.1088/2041-8205/807/2/L31 [arXiv:1505.05110 [astro-ph.SR]].
[3] T. Kuroda, T. Takiwaki and K. Kotake, Astrophys. J. Suppl. **222**, no. 2, 20 (2016) doi:10.3847/0067-0049/222/2/20 [arXiv:1501.06330 [astro-ph.HE]].
[4] B. Müller, T. Melson, A. Heger and H.-T. Janka, Mon. Not. Roy. Astron. Soc. **472**, no. 1, 491 (2017) doi:10.1093/mnras/stx1962 [arXiv:1705.00620 [astro-ph.SR]].
[5] C. D. Ott, L. F. Roberts, A. da Silva Schneider, J. M. Fedrow, R. Haas and E. Schnetter, Astrophys. J. **855**, no. 1, L3 (2018) doi:10.3847/2041-8213/aaa967 [arXiv:1712.01304 [astro-ph.HE]].
[6] E. O'Connor and S. Couch, Astrophys. J. **865**, no. 2, 81 (2018) [arXiv:1807.07579 [astro-ph.HE]].
[7] D. Vartanyan, A. Burrows, D. Radice, A. Skinner and J. Dolence, arXiv:1809.05106 [astro-ph.HE].
[8] H. Nagakura *et al.*, Astrophys. J. **854**, no. 2, 136 (2018) doi:10.3847/1538-4357/aaac29 [arXiv:1702.01752 [astro-ph.HE]].
[9] M. Oertel, M. Hempel, T. Klähn and S. Typel, Rev. Mod. Phys. **89**, no. 1, 015007 (2017) doi:10.1103/RevModPhys.89.015007 [arXiv:1610.03361 [astro-ph.HE]].
[10] R. B. Wiringa, V. G. J. Stoks and R. Schiavilla, Phys. Rev. C **51**, 38 (1995) doi:10.1103/PhysRevC.51.38 [nucl-th/9408016].
[11] J. Carlson, V. R. Pandharipande and R. B. Wiringa, Nucl. Phys. A **401**, 59 (1983). doi:10.1016/0375-9474(83)90336-6
[12] B. S. Pudliner, V. R. Pandharipande, J. Carlson and R. B. Wiringa, Phys. Rev. Lett. **74**, 4396 (1995) doi:10.1103/PhysRevLett.74.4396 [nucl-th/9502031].
[13] G. Audi, M. Wang, A. H. Wapstra, F. G. Kondev, M. MacCormick and X. Xu, Nucl. Data Sheets **120**, 1 (2014). doi:10.1016/j.nds.2014.06.126
[14] Koura H, Tachibana T, Uno M and Yamada M. 2005. Crossref:. doi:10.1143/PTP.113.305 Prog.Theor.Phys.,113,305-25
[15] K. Langanke and G. Martinez-Pinedo, Nucl. Phys. A **673**, 481 (2000) doi:10.1016/S0375-9474(00)00131-7 [nucl-th/0001018].
[16] K. Langanke *et al.*, Phys. Rev. Lett. **90**, 241102 (2003) doi:10.1103/PhysRevLett.90.241102 [astro-ph/0302459].
[17] T. Oda, M. Hino, K. Muto, M. Takahara and K. Sato, Atom. Data Nucl. Data Tabl. **56**, 231 (1994). doi:10.1006/adnd.1994.1007
[18] G. M. Fuller, W. A. Fowler and M. J. Newman, Astrophys. J. **252**, 715 (1982). doi:10.1086/159597
[19] T. Fischer, G. Martínez-Pinedo, M. Hempel, L. Huther, G. Röpke, S. Typel and A. Lohs, EPJ Web Conf. **109**, 06002 (2016) doi:10.1051/epjconf/201610906002 [arXiv:1512.00193 [astro-ph.HE]].
[20] S. Nakamura, T. Sato, V. P. Gudkov and K. Kubodera, Phys. Rev. C **63**, 034617 (2001) Erratum: [Phys. Rev. C **73**, 049904 (2006)] doi:10.1103/PhysRevC.73.049904, 10.1103/PhysRevC.63.034617 [nucl-th/0009012].
[21] H. Nagakura, K. Sumiyoshi and S. Yamada, Astrophys. J. Suppl. **214**, no. 2, 16 (2014) doi:10.1088/0067-0049/214/2/16 [arXiv:1407.5632 [astro-ph.HE]].
[22] H. Nagakura, W. Iwakami, S. Furusawa, K. Sumiyoshi, S. Yamada, H. Matsufuru and A. Imakura, Astrophys. J. Suppl. **229**, no. 2, 42 (2017) doi:10.3847/1538-4365/aa69ea [arXiv:1605.00666 [astro-ph.HE]].
[23] H. Nagakura, H. Ito, K. Kiuchi and S. Yamada, Astrophys. J. **731**, 80 (2011) doi:10.1088/0004-637X/731/2/80 [arXiv:1009.2326 [astro-ph.HE]].

[24] S. E. Woosley, A. Heger and T. A. Weaver, Rev. Mod. Phys. **74**, 1015 (2002). doi:10.1103/RevModPhys.74.1015